May 2020

Paper-Derived Ammonia Sensors Integrating A Natural Deep Eutectic Solvent

Makenzie Leigh Reynolds
Clemson University, kenzleigh97@gmail.com

PAPER-DERIVED AMMONIA SENSORS INTERGRATING A NATURAL DEEP EUTECTIC SOLVENT

A Thesis
Presented to
the Graduate School of
Clemson University

In Partial Fulfillment
of the Requirements for the Degree
Master of Science
Chemistry

---

by
Makenzie L. Reynolds
May 2020

Accepted by:
Carlos D. Garcia, Committee Chair
W. Bill Pennington
R. Kenneth Marcus

ABSTRACT

Ammonia is a naturally-occurring gas, present throughout the atmosphere at sub-ppb concentrations. As result of various processes, significantly higher concentrations can be found in the areas surrounding industrial and agricultural operations. In such cases, the presence of NH_3 in air not only is associated with a very pungent odor and potential toxicity but can also affect the environment, animals, plants, and humans. Aiming to provide a simple platform to monitor NH_3 in air, a paper-derived gas sensor, integrating a natural deep eutectic solvent (NADES) was developed. The herein described paper-derived ammonia gas sensor was fabricated using direct laser scribing, to form a carbon-based interdigitated array. Characterization and optimization (using chemometrics) were performed to develop a material with the lowest possible resistivity. A unique feature of the proposed sensor is that it integrates a natural deep eutectic solvent formed with lactic acid:glucose:water (LGH). This NADES conveys selectivity toward ammonia (over methanol, ethanol, 1-propanol, and water) and greatly enhances the sensitivity of the sensor (over the plain carbon array). The resistivity of the sensor was dependent on the NH_3 concentration in the 0.11 – 40.6 % range and has an estimated limit of detection of 0.11 %. Although the sensitivity of the sensor is lower than that of others based on metallic oxides, this approach represents a low-cost, portable, and simple way to detect and measure ammonia in gas phase.

TABLE OF CONTENTS

Page

TITLE PAGE i

ABSTRACT ii

LIST OF FIGURES iv

CHAPTER

I. INTRODUCTION 1-10

Ammonia 1
Why Ammonia Sensors? 2
Sensing Principles for Ammonia Sensors 3
Current Research 9

II. METHODS, RESULTS, AND DISCUSSION 11-29

Materials and Methods 11
Results and Discussion 15

III. CONCLUSIONS AND FUTURE RESEARCH 30-31

Conclusions of Paper-Derived Ammonia Gas Sensors 30
Future Research 30

REFERENCES 32

LIST OF FIGURES

Figure Page

1. Schematic design of the proposed interdigitated array for NH_3 sensing. The insert shows a photograph of a final device 13

2. Left: Scanning electron microscope image of the raw paperboard. Right: Scanning electron microscope image of the non-graphitizing carbon layer formed by pyrolysis with CO_2 laser 17

3. Scanning electron microscopy images of a side cut of the featured engraved (A) and the porous carbon layer (B) formed by laser engraving of cardboard. Conditions: 100 $mmol.L^{-1}$ borate, 66 $mm.s^{-1}$ speed and 8.4 W power 17

4. Scanning electron microscopy image of the cross section at high magnification of X250 18

5. Raman spectra of laser-scribed material fabricated using CO_2 laser power during the fabrication process and integration (D band area of 69690.57 and G band area of 57477.03) 18

6. There are three levels for each parameter in 3^3 Box-Behnken design: low (-1), medium (0) and high (+1). (A) Surface response with the change in power (W) and borate (mmol/L). (B) Surface response with the change in speed (mm/s) and borate (mmol/L). (C) Surface response with the change in power (W) and speed (mm/s). Resistance (Ω) was defined as response 21

7. (A) Response of sensor as a function of the pin width (mm) and (B) Response of sensor as a function of the pin-to-pin distance (mm) 23

8. (A) Dependence of the sensor's response as a function of the concentration of NH_3 and (B) Shows the linear range used to calculate the sensitivity and the limit of detection 25

9. Selectivity of the sensor towards ammonia and nitrogen saturated with methanol, ethanol, 1-propanol, and water, blank (air) also included 26

List of Figures (Continued)

Figure Page

10. Stability of sensor toward 40.6% NH_3 27

11. TGA experiment with NADES 28

12. Sensor response toward Halibut as a function of storage time at 25°C. 29

CHAPTER ONE

INTRODUCTION

1. Ammonia

While the concentration and chemical structure of the compounds involved in poultry and fish production can be extremely diverse,[1] most of them result from the decomposition of organic matter, including food, manure, and waste products. Among those, volatile carboxylic acids, thiols, and amines (including ammonia, NH_3) are the most relevant. For many industries, the release of NH_3 is one of the most important issues not only because of the pungent odor and environmental impact of the gas but also because it affects production levels in farms because such high levels of NH_3 being produced cause companies to slow production to lower NH_3 levels to a safe concentration. Also, the concentration of NH_3 affects the animal health due to prolonged exposure to concentrations as low as 20 ppm. [2] Exposure to high levels of NH_3 gas can lead to life-threatening illnesses in humans due to the highly corrosive properties and toxicity levels. Occupational Safety and Health Administration (OSHA) have stated that the exposure limit for humans to NH_3 is eight hours at a concentration of 25 ppm or just ten minutes at concentrations higher than 35 ppm.[3,4]

NH_3 is emitted daily into the atmosphere, accounting for an annual release of 2.0 – 8.0 Tg of NH_3 due to human activity.[5] Beyond the naturally-present concentrations around the part-per-billion (ppb) range,[6] NH_3 is known as an environmental pollutant. Due its reactive properties, ammonia is able to react with nitric or sulfuric acid and form ammonium nitrate and ammonium sulfate, which are also highly toxic.[7] These compounds,

often present in the form of aerosols, contribute to the formation of smog, further effecting the atmosphere and potentially leading to increases in the global temperature.[8,9] Regardless of the source, NH_3 also participates in a number of natural processes in the atmosphere. The process starts with the atmospheric nitrogen, that goes through nitrogen fixation via bacterial conversion.[10] The next process is nitrification, where a nitrifying bacterium converts the ammonium into nitrites.[11,12] The nitrites are then used by plants as nutrients. After the plants die, decomposer bacteria or fungi converts the nitrites back into ammonium, through a process called ammonification.[13,14] Finally, bacteria is able to convert ammonium back to nitrogen gas and release it into the atmosphere, through a process called denitrification. While NH_3 is not considered a greenhouse gas, NH_3 does indirectly attribute to nitrous oxide (N_2O) emission,[15] which is a known greenhouse gas.[16] Nitrous oxide can also be produced through the denitrification process.[17] Other sources of NH_3 come from combustion, industrial releases, and fertilizers.[18]

2. Why Ammonia Gas Sensors?

While the human nose is able to sense high concentrations of NH_3 in the air due to the penetrating odor it carries, determining lower concentrations is more challenging.[19] There are many different areas and industries that have a need to detect and measure NH_3 in the low concentration range, including automotive, chemical, and environmental. As previously mentioned, NH_3 is able to form aerosols that are very harmful to the environment.[20–22] Automotive industries need to be able to detect atmospheric pollutants like NH_3 for air quality control inside cars.[23] Sensors have been developed for these systems

so when there is low air quality, the valves that pull air from outside the car are able to close so the contaminated air doesn't get inside the car.[24–26] NH_3 is also chemically made in mass quantities due to the high demand from fertilizer companies and chemical production, potentially leading to small leaks.

The maximum amount of NH_3 that is allowed in a workspace, with long-term exposure is 20 ppm. As a point of reference, and while most industries are not required to have fast detection sensors, air in farming areas can contain levels twice as lower than what is allowed in a workspace .[27] As such, there is a major need to monitor the concentration of the NH_3 in these areas to ensure that neither animals nor people are exposed.[27]

3. Sensing Mechanisms for Ammonia Gas Sensors

There are many different sensing principles that can be used in NH_3 detection and measurements which depends on the application of the sensor. Many times, the different principles can be categorized into three groups, which are optical (tunable diode laser spectroscopy[28]), solid-state (conducting polymer[29,30] and metal oxide[31,32]), and other (electrochemical[33]) sensing methods. These different principles provide specific solutions to a wide variety of applications and typically are able to address different monitoring needs.

3.1 Optical Sensing Methods

Optical gas sensors are widely accepted in commercial settings due to the low cost, fast analysis, long lifetime, and simplicity.[34] Another advantage of this method is its ability

to operate under many different temperatures.[35] These sensors can collect information simultaneously on the intensity and wavelength.[36] Gas sensors using optical absorption are also frequently used, especially the tunable diode laser absorption spectroscopy (TDLAS) method.[20,35] In this technique, the detection is based on the absorption in the infrared spectral region. Thus, TDAS is able to detect multiple analytes in gas phase. For NH_3, the typical wavelength spectrum range that is used is 1450 to 1560 nm[37] and the instrument typically includes the laser, a photodetector, an analyte gas chamber, a reference chamber, a control unit for temperature and pressure, and an analyzer for the electronics.[35,38,39] Even though there are many advantages to using this technique, such as high sensitivity, selectivity, simple operation, and noninvasive detection[40], cryogenic temperatures and high current are needed to be able to confine carriers to the junction region because there is a large loss during operation, which are a major disadvantage.[40] To address these, advanced diode laser sources[41] were developed. Among others, quantum cascade lasers (GCLs) were found to be a better option for the diode laser source to enhance TDLAS system, as they were able to operate at room temperature, and provide selectivity, high resolution and sensitivity.[42–44] With the use of QCL, Tao et al. fabricated an open-path mobile sensing platform for measurements of greenhouse gases and air pollutants.[45] They were also able to develop a mobile sensing system that could be attached to the roof rack of a car to monitor the gases in different areas in the city.[45] This could be helpful to determine if some areas are releasing more pollutants than others and construct a plan to lower the pollutants being let into the atmosphere.

3.2 Solid-State Sensing Methods

There are two main types of solid-state methods used for NH_3 detection, including those based on conducting polymers and metal oxides. There are several different types of polymers that are used in gas sensing, such as polyaniline, polythiophene, and polypyrrole. These are just some of the more popular polymers but there are many more than just three mentioned here.[6,46,47] With these conducting polymers sensors, there are many different options for the operation method, including potentiometric, colorimetric, conductometric, and amperometric.[35,48] The most common method used is amperometric by using the redox reaction between the conducting polymer and specific gas.[49] Conducting polymers have several advantages when being used as the sensing principle in gas sensors, including stability, easy fabrication, tunability, and flexibility. With all of the advantages, there are some disadvantages as well. The main disadvantage is the low sensitivity of the conducting polymer.[50] To enhance the sensitivity of the sensors, modification of the structure of the polymer and using dopants was proposed. It was found with modification of the polymer; the sensing properties were significantly improved due to facilitation of proton or electron transfer and giving a better interaction between the analyte gas and the sensing film. With dopants added, it was found to improve the sensitivity by providing higher surface area for molecules to diffuse onto the sensing film.[51] Du et al. reported enhanced polyaniline (PANI) nanofibers showing enhanced sensing performance towards NH_3 by looking at the deprotonation rate. They found that the improved sensitivity and response could be due to the NH_3 molecules being able to diffuse into the PANI film and react with the PANI chains on the active site due to the small diameter size which results into a large specific area.[52]

Andre et al. also reported a NH_3 gas sensor composed of zinc oxide nanofibers (ZnO) decorated with poly(styrene sulfonate) (PSS) with enhanced sensitivity.[53] The group compared the sensitivity of the sensor with pure ZnO nanofibers without PSS and with PSS. It was found that the pure ZnO nanofibers with no PSS decorated showed quite a low response to NH_3 gas compared to the ZnO fibers decorated with PSS which showed a much higher response. The added PSS increased the response to NH_3 gas significantly, they accounted this to the high surface area the dopant adds to the sensing film.[53]

In recent years, metal oxide-based sensors have become very popular for gas sensing due to the low-cost and flexibility of the fabrication process as well as the simplicity of the resulting sensors.[35] These materials (especially if formulated in their nanostructured forms) provide unique features due to their mechanical, electrical, magnetic, and operational properties.[54] There are many different types of metal oxides that are used in gas sensing, some of the most popular ones used for NH_3 gas sensors are ZnO, TiO_2, SnO_2, and MoO_3.[55–57] Most often, the double-Schottky barrier is used as a model by looking at the grain boundaries to explain the sensing mechanism behind the metal oxide-based sensors. At the grain boundaries of the potential barrier, due to the charged atmospheric oxygen molecules, there is an increase in the height of the barrier that form a depletion layer. This happens because the electrons are trapped onto the surface of the metal oxides, which results in a decrease in the conductivity. The opposite occurs when a reducing gas, such as NH_3, introduced to the sensing film, where the height of potential barrier decreases, increasing the conductivity.[35] There are many advantages to these sensors, including low cost, flexible fabrication, and simplicity. Even with these

advantages, there are always disadvantages which (in this case) include low selectivity. To enhance the selectivity of these sensors, a second phase material was added to the metal oxide surface and investigated to regulate the conductivity of the metal surface.[58] Zeng et al. was able to show that adding a second phase material to the metal oxide surface does improve the selectivity of sensor towards NH_3.[59] The sensor developed was fabricated from Pd-sensitized ZnO nanostructures. This second phase, palladium, provided better selectivity towards NH_3 and faster response than the pure ZnO. The authors attributed the enhanced response of the Pd-sensitized ZnO to the formation of weak-bonded complexes between the oxygen molecules and the palladium atoms. This complex is able to capture more electrons at the surface of the grains to form more oxygen species which gives a better response to NH_3.[59] Another group, Zhang et al., developed a MoS_2/Co_3O_4 nanocomposite film sensor that was able to yield enhanced sensing performance towards NH_3. They wanted to show the effects of adding more than one self-assembled layer of molybdenum disulfide to the tricobalt tetraoxide nanorod. To do this, they looked at the response of one, three, five, and seven layers to different concentrations of NH_3. It was found that adding multiple layers gave an increased response up to five layers then after the seventh layer the response started to decrease again. This was found to be due at low amounts of layers, that there is not enough conductivity to give a high response and with more layers than five, gas diffusion started to become more difficult resulting in a decrease in response at seven layers.[60]

3.3 Electrochemical

Electrochemical gas sensors have become more popular lately due to the many advantages they provide including portability, cost-effectiveness, and low power use. These sensors are also known to have high sensitivity towards analytes in gas phase. Most electrochemical gas sensors have the same basic set up, including the counter electrode, sensing electrode, reference electrode, a gas permeable membrane, and an electrolyte.[61] Electrochemical gas sensors can be classified according to the electrolyte used being either solid or liquid state electrolytes. Specifically, solid-state use electrolytes use potentiometric and amperometric techniques and liquid-state electrolytes use voltammetric techniques.[62] In electrochemical NH_3 gas sensors, potentiometric techniques are often used for the sensing mechanism. This sensing mechanism works by measuring the difference in the electrical potential between the sensing and counter electrode. This happens as the NH_3 gas is diffusing across the gas permeable membrane.[63] These sensors rely on the function of the electrolyte, which is why problems with the electrolyte can cause many issues with an electrochemical gas sensor. Alternative electrolytes have been studied to improve the problems traditional electrolytes have, including large consumption of the electrolyte from each detection which reduces the lifespan of the sensor. One of the most popular alternative electrolytes being studied is room temperature ionic liquids (RTILs). RTILs have superior electrochemical range, can stay at a liquid state for a range of temperatures, and exhibit a wide potential window.[64,65] Sekhar et al. developed an electrochemical NH_3 gas sensor on a paper substrate. The sensor was fabricated using RTILs as the electrolyte with a platinum electrode.[66] The paper substrate was used due to the low cost and simplicity. The sensor showed high sensitivity and selectivity toward NH_3 gas.[66]

4. Current Research

To address the limitations, the presented research is on the development of a paper-based chemiresistive NH_3 sensor integrating a natural deep eutectic solvent. The sensor is fabricated using the direct laser scribing method developed by Araujo.[50] This laser scribing method utilizes the high temperature of the laser which causes the formation of conductive, porous carbon which can be used to perform electrical measurements. There are many advantages to this technique which include a simple and easy procedure, no harsh chemicals used, and controlled gas conditions are no longer needed.[50] To give the sensor selectivity towards NH_3, natural deep eutectic solvents (NADES) were used as the sensing film. The selected NADES (called LGH^{67}) was prepared from a mixture of lactic acid (L) and glucose (G) with a 5:1 ratio with 15 % of H_2O (v/v) (H). The selected NADES would act as an electrolyte connecting the pins in the array, and where the glucose (weak hydrogen bond acceptor) could be displaced by ammonia (strong hydrogen bond acceptor), changing the availability of the protons released by the lactic acid, and leading to an increase in the resistivity of the system. The sensing film is deposited onto the paper substrate to allow detection and quantification of the gas analyte. To acquire these green solvents, a hydrogen-bond acceptor is mixed with a hydrogen bond donor molecule which leads to a notable decline of the melting point as the when combined the melting point is lower than either of the two constituents. The main driving force in the formation of the NADES is hydrogen bonding which play a major role in the characteristics of the mixture. There are many advantages of NADES which include low toxicity, sustainability, easy preparation,

large ionic conductivity, wide electrochemical window, and a larger number of combinations can be made.[67] A new method of preparation has been developed using microwave radiation (MW) to optimize the energy consumption being used. Microwave radiation has been found to be more environmentally friendly by having shorter reaction times and higher yields.[68] This method is faster, cheaper, greener, and easier than any of the other top methods that have been used in the past.[69] With the use of NADES for gas sensing, we developed a simple, cost- effective, and portable paper-based NH_3 gas sensor based on the direct laser scribing process.

CHAPTER TWO

METHODS, RESULTS, AND DISCUSSION

1.1. Reagents

Ammonium hydroxide was purchased as 28-30% w/w (J. T. Baker, Phillipsburg, NJ) and when needed, diluted with deionized water (Milli-Q, Millipore Water Systems; Billerica, MA, USA). The borate solution was prepared by dissolving sodium tetraborate decahydrate (Acros Organics, Geel, Belgium) in deionized water. A solution of chitosan (Sigma Aldrich, St. Louis, MO, USA) was prepared using 300mM acetic acid, and used to adhere the formed carbon and give mechanical stability to the sensor. Methanol and ethanol were purchased from VWR International (Radnor, PA, USA). 1-propanol was purchased from Alfa Aesar (Ward Hill, MA, USA). Compounds for the preparation of the NADES included anhydrous glucose (≥ 99%) and L (+) lactic acid (85%-90%), both purchased from Sigma Aldrich (St. Louis, MO, USA). The paperboard (thickness = 1.27 mm, 800 $g.m^2$) used for fabricating the sensor was purchased from Logic Dealz (via amazon.com).

1.2 Fabrication of Paper-Based Chemical Sensor/Array.

Although there are many alternatives to deposit electrodes on paper (including screen printing,[70] drop casting,[71] and inkjet printing,[72]) one of the simplest approches is laser engraving.[73,50] In this case, the device was first designed in CorelDraw X (Ottawa, ON) and then transferred to the engraver. Prior to the fabrication of the sensor, the paperboard was soaked in a solution containing 0.1 mol L^{-1} sodium borate for 10 minutes and then left to dry overnight. The borate acts as a flame retardant, decreasing the amount

of material ablated during the engraving process[74,75] and promoting to formation of char (instead of tar[76]). The sensor was then engraved onto the paperboard using an Epilog Mini Laser Engraver (Golden, CO), equipped with a 30 W CO_2 laser. This laser engraver has two engraving modes: raster and vector. These modes are typically used for marking or cutting the material, respectively. To fabricate the interdigitated array and pads for electrical connections, the laser was set to the raster mode, moving at a lateral speed of 66 mm/s (4 % of 1650 mm/s)[77] and a power of 8.4 W (28 % of 30 W), performing two passes over the same surface, leading to a uniform layer of carbon. The sensor was then cut out using the vector mode (247.5 mm/s and 25.5 W). To preserve the pyrolyzed material, the sensor was then immersed in a chitosan solution for one minute and then dried in a convection oven (85 ^{o}C) for ten minutes. As the last steps, a silicon barrier (GE Advanced Silicon) was deposited on each side of the array (to keep the NADES in the middle of the array) and electrical contacts were added using silver paint (SPI Supplies; West Chester, PA, USA). Figure 1 shows a schematic representation of the arrangement of the elements and selected geometry for the paper-derived sensor.

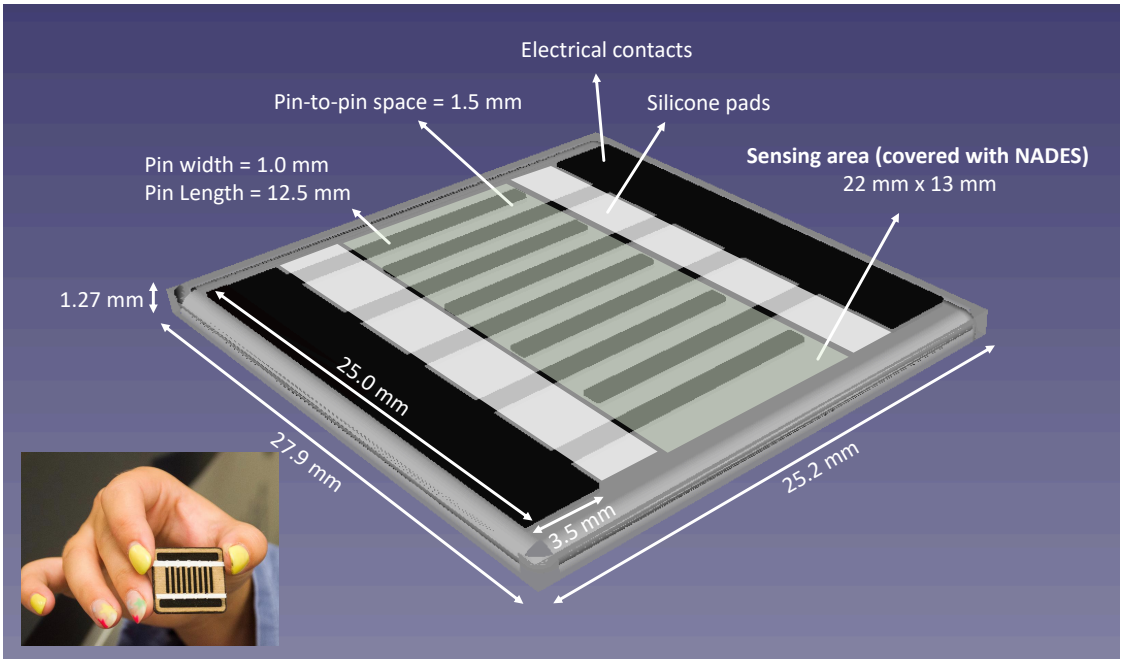

Figure 1: Schematic design of the proposed interdigitated array for NH_3 sensing. The insert shows a photograph of a final device.

*1.3 Characterization of the material***.**

Scanning electron microscopy (S3400 and SU6600, Hitachi High Technologies, Pleasanton, CA) images were obtained to compare changes in the physical structure of the material as a result of the engraving process. Raman spectra were excited with 514.5 nm light from an Ar^+ ion laser (Innova 200, Coherent, 500 mW). Scattered light was collected by a f/1.2 camera lens (Nikon) in a 45° backscattering geometry and analyzed by triple spectrometer (Triplemate 1877, Spex) equipped with CCD camera (iDUS 420, Andor). The spectral resolution at the excitation wavelength was 0.2 nm. Raman spectrum of indene was used for the spectral calibration.

1.4 Selection and Preparation of the NADES.

The selected NADES (called LGH)[67] was prepared from a mixture of lactic acid (L) and glucose (G) with a 5:1 ratio with 15 % of H_2O (v/v) (H). This NADES was selected because it features low vapor pressure, high viscosity, and its high polarity is relatively constant in a wide range of water contents (44.8 $kcal.mol^{-1}$), maintaining its supramolecular structure throughout the experiment. The selected NADES acts as an electrolyte connecting the pins in the array, where the glucose (weak hydrogen bond acceptor) could be displaced by ammonia (strong hydrogen bond acceptor), changing the availability of the protons released by the lactic acid, and leading to an increase in the resistivity of the system. For these experiments, the LGH was synthetized using the microwave assisted method, as recently described by Silva and co-workers.[69] Briefly, all components were mixed in a glass vial and then heated in a microwave (power set at 100 W) for 10 s, leading to the formation of the liquid eutectic system. The NADES was then allowed to cool down to room temperature and was ready to use. In all cases, 100 μL of the NADES were placed in the middle of each sensor (see Figure 1, 22 mm x 13 mm) and allowed to soak through the paperboard for 20 min before performing any experiments.

1.5 Cell Set-Up.

In order to control the atmosphere of the sensor, a chamber of 76.2 mm x 127.0 mm x 50.8 mm was fabricated using 3 mm-thick acrylic. The material was also cut using the laser engraver on the vector setting at 165 mm/s (10 % speed), 30 W (100 % power), and a frequency of 5000 Hz. Next, the box was assembled and glued together using a few

drops of dichloromethane on each edge, to dissolve a thin layer of the material and permanently attach them. The top layer of the box was left unglued to allow replacing the sensor. Two holes were cut out on the ends of the box to attach inlet and outlet gas lines. Also, two smaller holes were made on the opposite sides of the box to make the electrical connections between the sensor and the multimeter (Fluke 115 digital multimeter; Fluke, Everett, WA). In order to deliver a known concentration of ammonia (gas) to the sensor, a stream of N_2 was bubbled (at 1 $sl.min^{-1}$) through an aqueous solution (10 mL, using a 50 mL Falcon tube) containing a known concentration of NH_4OH. The concentration of NH_3 in gas phase was presented in % to be able to compare results to other NH_3 gas sensors. The concentration was calculated by titrating the NH_3 captured in DI water from the bubbling system with H_2SO_4.[33] For the other gases, the corresponding saturation vapor pressure for methanol (13 kPa), ethanol (5.9 kPa), 1-propanol (3.2 kPa), or water (2.0 kPa) was used.[78] This approach has been used multiple times before and represents a safer and more convenient alternative to having NH_3 cylinders.[79–81]

2. Results and Discussion

2.1 Characterization of Paper-Derived Material.

The selected paperboard is composed of cellulose and other materials like $CaCO_3$[82] and kaolin,[83] commonly used as additives. Upon thermal treatment, the cellulose is transformed into carbon via though a number of sequential reactions involving depolymerization, formation of anhydrosugars, furans, glycolaldehydes, and condensation reactions.[84,85] The material formed features electrical conductivity, porous

structure, and good mechanical stability.[86] To confirm the structural change that occurs after thermal treatment by the CO_2 laser-scribing process, the topography of both the raw paperboard and laser-scribed paperboard were investigated via scanning electron microscopy (SEM). As it can be observed in Figure 2 (left), the raw paperboard was composed of large cellulose fibers (53 ± 12 μm in diameter, n=5) that are entangled together. On the other hand, the carbon material formed by the laser-scribing process features thinner fibers (24 ± 3 μm, n=5, Figure 2, right), that preserve the overall random structure of the original material. It is also important to mention that although the pyrolysis of plain paper can lead to the formation of a number of structures (fibers, particles, and foam-like structures), engraving the borate-soaked paper leads to the formation of a porous non-graphitizing carbon material with high-surface area (Figure 3) considered appropriate for the development of gas sensors. SEM images were also used to calculate the depth of the engraved features (removed material, 480 ± 20 μm, n=5) and the thickness of the carbon material forming the pins (170 ± 10 μm, n=5) formed by laser engraving of the paperboard (Figure 4). To confirm the formation of the carbon layer and determine the composition of the material, the engraved paperboard was interrogated by Raman spectroscopy. As it can be observed in Figure 5, two clear bands (attributed to disordered and graphitic structures) appeared around 1345 and 1585 cm^{-1}, respectively. The ratio of the areas in each peak was calculated to be 1.212 (seen in Figure 5, right), value that is in line with other cellulose-derived carbon materials prepared by pyrolysis.[50]

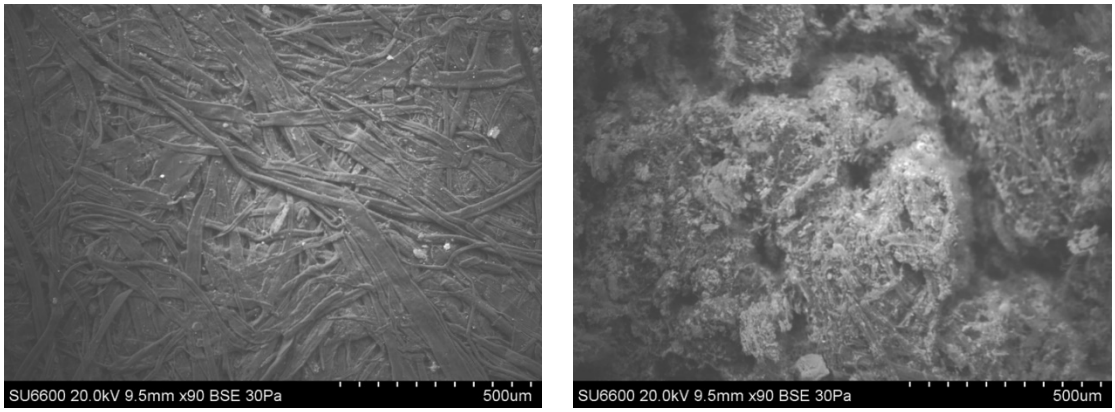

Figure 2: Scanning electron microscopy image of the paperboard before (left) and after the pyrolysis with CO2 laser (right)

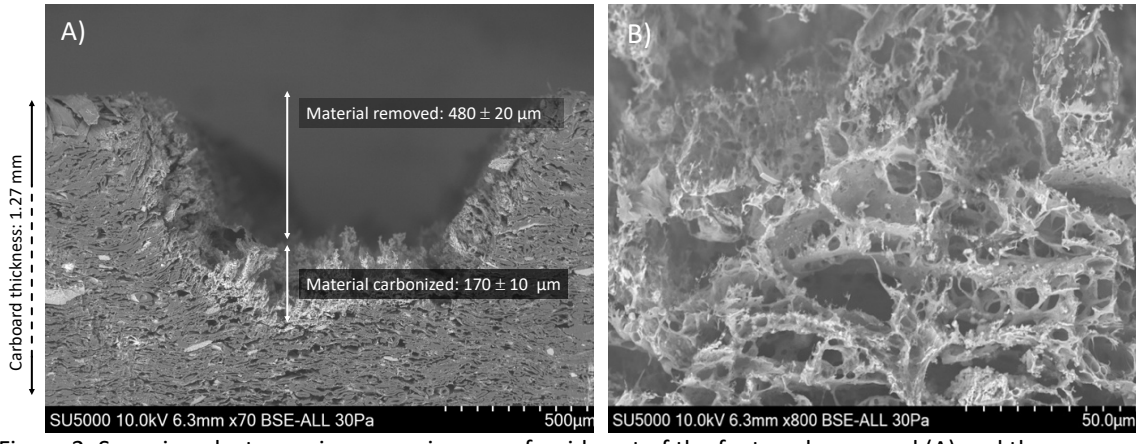

Figure 3: Scanning electron microscopy images of a side cut of the featured engraved (A) and the porous carbon layer (B) formed by laser engraving of cardboard. Conditions: 100 mmol.L^{-1} borate, 66 mm.s^{-1} speed and 8.4 W power.

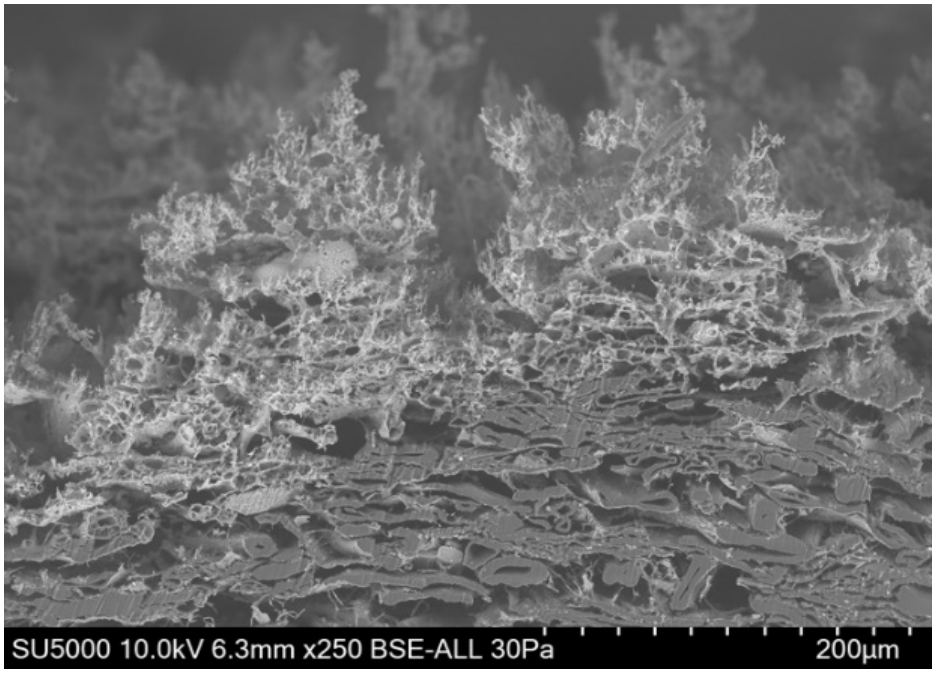

Figure 4: Scanning electron microscopy image of the cross section at high magnification of 250.

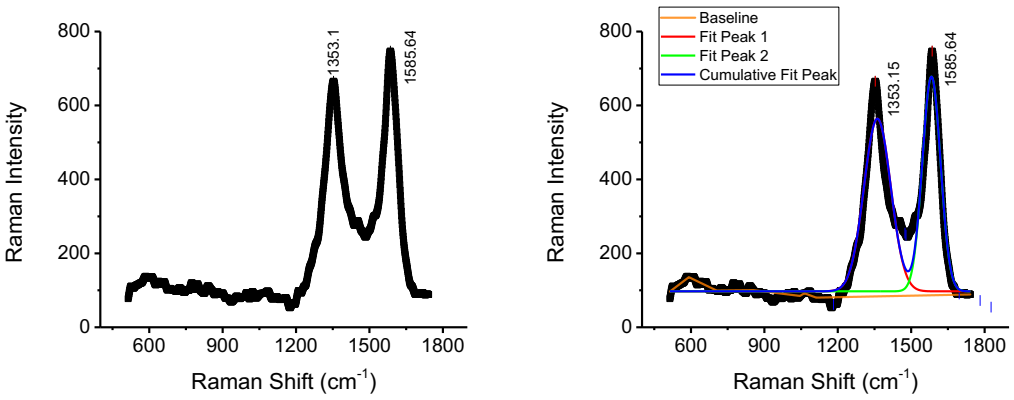

Figure 5: Raman spectra of laser-scribed material fabricated using CO2 laser power during the fabrication process and integration (D band had an area of 69690.57 and G band had an area of 57477.03)

These preliminary results were used as the starting point to develop the matrix used to optimize the conditions leading to a material with the lowest possible resistivity.

2.2 Optimizing the Fabrication of the Paper-Derived Material and Architecture of the Sensor.

Based on preliminary results, it was determined that several variables linked to the fabrication of the material would affect its electrical conductivity and (in turn) the response of the sensor. Among those, the variables that had the largest effect on the signal were the concentration of borate used to soak the paperboard, the incident power, and the engraving speed. Therefore, and with the objective of identifying the experimental conditions leading to the material with the lowest resistance, a chemometric approach was implemented. Using preliminary results, the low, medium, and high values were selected for borate concentration (100 $mmol.L^{-1}$, 200 $mmol.L^{-1}$, and 300 $mmol.L^{-1}$), power (6.0 W, 7.5 W, and 9.0 W), and lateral speed (66.0 $mm.s^{-1}$, 82.5 $mm.s^{-1}$, and 99.0 $mm.s^{-1}$). It is important to mention that for the case of power and lateral speed, the limits of the variables were defined by the amount of material pyrolyzed and/or removed during the engraving process. In other words, outside the selected ranges the laser was either not able to form carbon or able to penetrate the entire thickness of the paperboard. With this in mind, a matrix was developed following the 3^3 Box-Behnken design that consisted of 15 experiments, with genuine triplicates at central point. The experiments were randomly performed to eliminate bias and distribute the errors throughout the experimental landscape using the resistance of the material as the performance metric. It is important to mention that because different

engraving conditions would lead to different thickness values of the carbon formed, the resistance (measured using as-prepared substrates, 3.0 mm in width and over a distance of 5.0 mm) was selected over the resistivity of the material. As shown in Figure 6A, where the resistance of the material is analyzed as a function of the incident power (W) and borate concentration ($mmol.L^{-1}$), the lowest resistance was achieved at the mid-level power and high-level borate concentration. As shown in Figure 6B, where the resistance of the material was analyzed as a function of the lateral speed ($mm.s^{-1}$) and borate concentration ($mmol.L^{-1}$), the lowest resistance of the material was obtained at low-level speed and either low or high-level borate concentrations. As shown in Figure 6C, where the resistance of the material was analyzed as a function of the incident power (W) and lateral speed ($mm.s^{-1}$), the lowest resistance of the material was obtained combining mid-level power and low-level speed. Based on these surface response graphs, the lowest borate concentration (100 $mmol.L^{-1}$, marginal effect), the lowest lateral speed (66.0 $mm.s^{-1}$) and a mid-level incident power were selected as the optimum conditions to form a material with the lowest resistance. It is also important to mention that the power selected as optimum for the fabrication of the sensors (8.4 W) was selected after performing a few additional experiments around the initial middle range of power (7.5 W), but maintaining a fixed borate concentration and speed.

A)

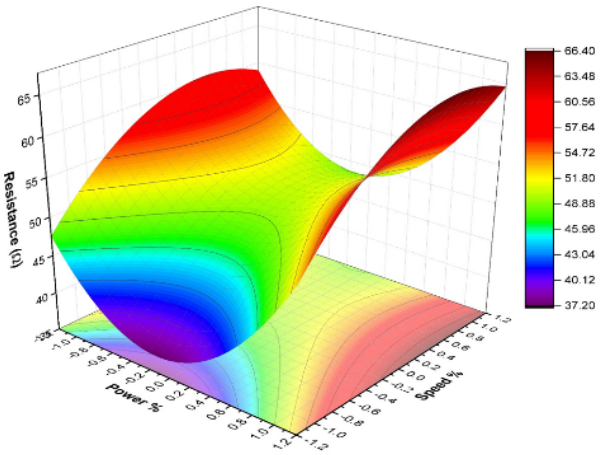

B)

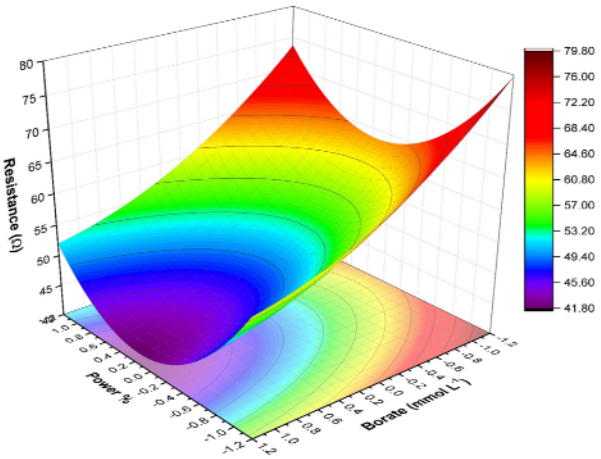

C)

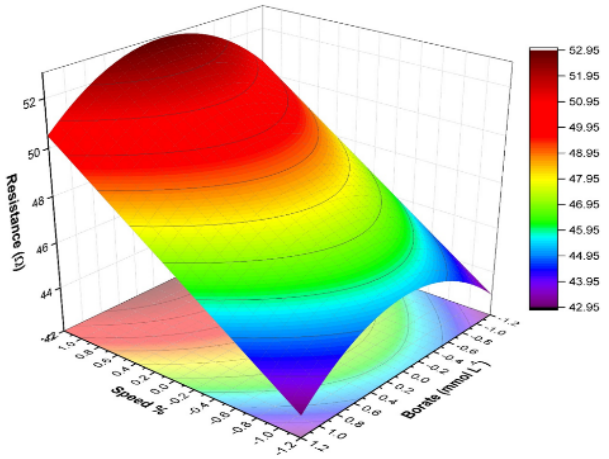

Figure 6: There are three levels for each parameter in 3^3 Box-Behnken design: low (-1), medium (0) and high (A). (A) Surface response with the change in power (W) and borate (mmol/L). (B) Surface response with the change in speed (mm/s) and borate (mmol/L). (C) Surface response with the change in power (W) and speed (mm/s). Resistance (Ω) was defined as response.

Next, the effects of the pin width and pin-to-pin distance on the response of the sensor were investigated in the 0.5 to 2.0 mm and 1.0 to 2.5 mm range, respectively. These ranges were selected considering the resolution of the engraver, the number of pins in the array, and the overall size of the resulting sensor. For these experiments, the response of the sensor ($\Delta\Omega$) was calculated by subtracting the resistance measured in the presence of NH_3 vapor minus the resistance measured during baseline stabilization (bubbling N_2 in water). For these experiments, 100 μL of the selected NADES were dispensed to cover the sensing region of the array. It is also important to note that control experiments performed without the addition of the NADES rendered no changes in the resistance of the array upon the introduction of the NH_3 (data not shown). This behavior was attributed to the capacity of NH_3 (weak base that behaves as a proton acceptor)[87] to compete for the proton released by the lactic acid, thus affecting the conductivity of the interdigitated array.

Figure 7A summarizes the results obtained when the response of the sensor was investigated as a function of the pin width. From the figure, it can be observed that the sensor shows the highest response at a pin width of 0.5 mm but considering the size large variability of the signal obtained with this value (represented by the error bar) and the overall size of the array, a pin width of 1.0 mm was chosen for the final gas sensor fabrication. In Figure 7B, the response as a function of the pin-to-pin distance is summarized. In this case, the larger the gap between the pins, the highest the response obtained. This behavior was attributed to the fact that such distance defines the active area

of the sensor to capture NH_3. Again, considering the variability of the signal (large error bars) and the overall size of the array, a pin-to-pin distance of 1.5 mm was selected as optimum. Summarizing, from these experiments, the final configuration for the sensors was selected to be 9 pins, with a width of 1.0 mm and a pin-to-pin distance of 1.5 mm. While not considered within the scope of the current study, it is noted that increasing the number of pins (and the size of the device) could lead to increases in the sensitivity of the sensor.

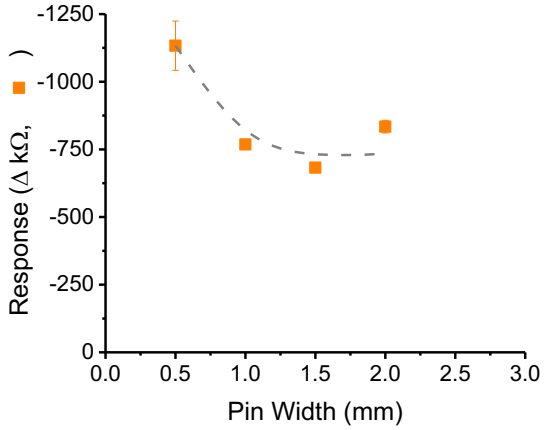

Figure 7A: Response of sensor as a function of the pin width. Conditions: 100 mmol.L^{-1} borate, 66 mm.s^{-1} speed and 8.4 W power, pin-to-pin distance: 1.5 mm, 40.6% NH_3, carrier flow rate: 1 sl.m^{-1}, room temperature.

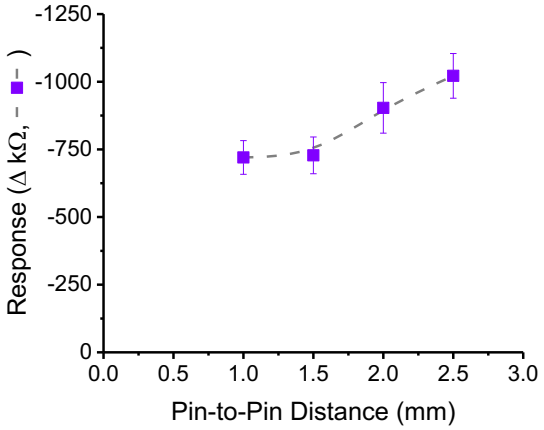

Figure 7B: Response of sensor as a function of the pin-to-pin distance (mm) Conditions: 100 mmol.L^{-1} borate, 66 mm.s^{-1} speed and 8.4 W power, pin width: 1.0 mm, 40.6% NH_3, carrier flow rate: 1 sl.m^{-1}, room temperature.

2.3 Sensitivity.

In order to determine the analytical figures of merit, the response of sensor was investigated using solutions containing different concentrations of NH_4OH, leading to different partial pressures of NH_3 in the gas phase. For each measurement, the sensor was placed inside the cell and attached to the multimeter. Then, N_2 was bubbled through a solution containing only water, to allow stabilizing the baseline. Next, the water solution

was replaced by one with a known concentration of NH_4OH and the bubbled through N_2 was injected into the chamber with the sensor. The NH_3 vapor was left flowing through the chamber until the resistance stabilized (typically within 20 min), but the amount of time required was dependent on the concentration of NH_3 (higher concentration required shorter stabilization times). Subsequently, the sensor was allowed to recover with background gas (N_2 bubbled through water) until the resistance stabilized.

To investigate the response of the sensors to the concentration of NH_3, aqueous solutions containing NH_4OH in the 0.06 mol L^{-1} to 17.6 mol L^{-1} range were used, leading to gas phase concentrations in the 0.11% – 40.6% range, respectively. The results are summarized in **Error! Reference source not found.**A, where datapoints and the error bars represent the average and standard deviation, respectively, obtained with three measurements. As it can be observed, the sensor displayed a typical response, where initial increases in the NH_3 concentration (in the 0.11 % to 3.40 % range) lead to significant increases in the response. However, concentrations above 3.40% only led to marginal changes in the response, behavior that was attributed to the saturation of the sensor and that is commonly found in the literature.[81,88] Figure 8B shows the linear range used to calculate the limit of detection (0.11%, S/N=3) of the device. These figures are comparable to those previously reported for a Ag-based sensor[89] but higher than most sensors, including those reported by King et al.,[33] Vaughan et al.,[90] and Shang et al.[91]. While the low sensitivity of the sensor limits its potential deployment for environmental and human safety applications, these simple and

low-cost sensors could be used for a number of industrial applications (feed lots, poultry farms, etc).

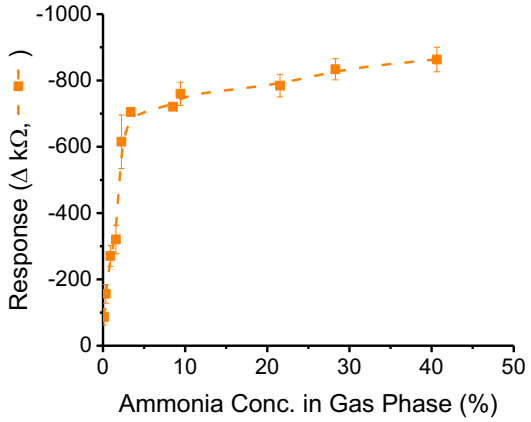

Figure 8A: Dependence of the sensor's response as a function of the concentration of NH_3. Conditions: 100 $mmol.L^{-1}$ borate, 66$mm.s^{-1}$ speed and 8.4W power, pin-to-pin distance: 1.5 mm, pin width: 1.0 mm, carrier flow rate: 1 $sl.m^{-1}$, room temperature.

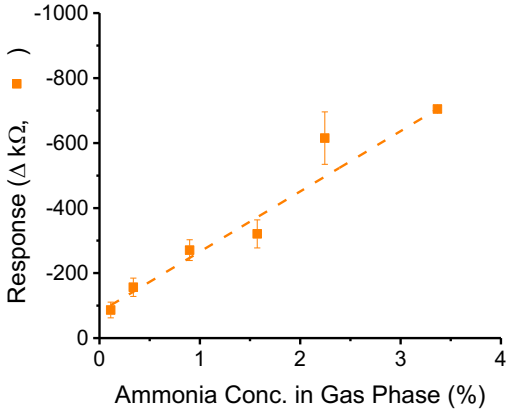

Figure 8B: Shows the linear range, used to calculate the sensitivity and limit of detection of the device. Conditions: 100 $mmol.L^{-1}$ borate, 66$mm.s^{-1}$ speed and 8.4W power, pin-to-pin distance: 1.5 mm, pin width: 1.0 mm, carrier flow rate: 1 $sl.m^{-1}$, room temperature.

2.4 Selectivity, Stability and Temperature.

Selectivity, stability, and temperature are critical characteristics for gas sensors and need to be investigated thoroughly. Thus, the selectivity of the paper-derived gas sensor was studied measuring the response when the sensor was exposed to ethanol, methanol, 1-propanol, and water. These compounds were selected because they can function as both a weak bases (proton acceptor) and (very) weak acids (proton donor, pKa values ranging from 14 to 16).[92] The results are summarized in Figure 9, where the response of the sensor to 4.0.6% NH_3 (solution containing 30% w/v NH_3), methanol (98%, 13%), ethanol (98%, 5.8%), 1-propanol (98%, 3.2%), and water (2%) is shown. The results show that while the

sensor was able to respond to NH_3, it only showed marginal responses to ethanol, methanol, or water. As a point of reference, and without considering the differences in concentration, the signal for NH_3 was fivefold higher than that of the other analytes at saturation concentrations.

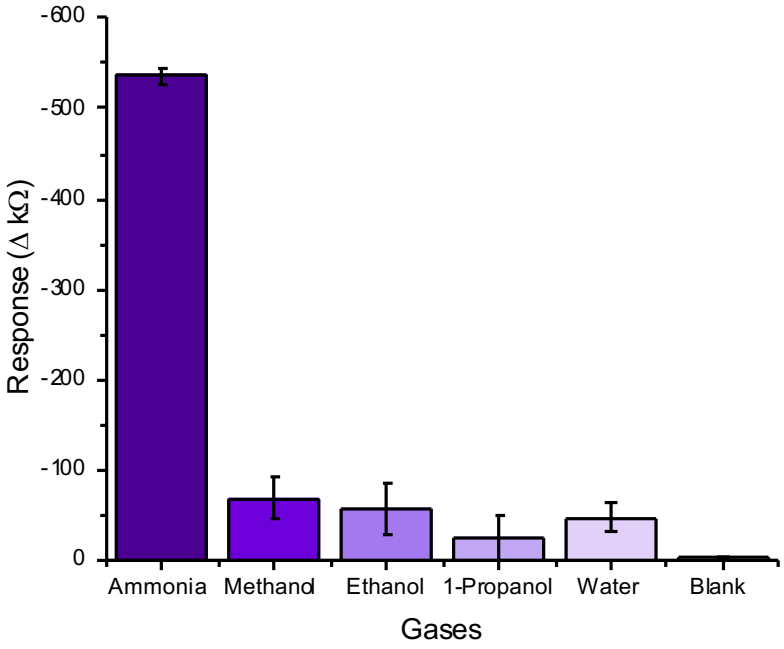

Figure 9: Selectivity of the sensor toward NH_3, methanol, ethanol, 1-propanol, water, and air (blank). Conditions: 100 mmol.L^{-1} borate, 66mm.s^{-1} speed and 8.4W power, pin-to-pin distance: 1.5 mm, pin width: 1.0 mm, carrier flow rate: 1 sl.m^{-1}, room temperature.

Secondly, the investigation of the long-term stability of the sensor was conducted by measuring the response of the sensor with 40.6% NH_3 in the gas phase for 18 days at room temperature. The measured results, in Figure 10, reveal there was only a minor fluctuation in the sensing responses observed during the 18-day period. This shows that the sensor possesses a stable response to NH_3 gas. This sensor has shown to have good stability over

an 18-day period, but it could also be used as a disposable sensor due the low fabrication cost.

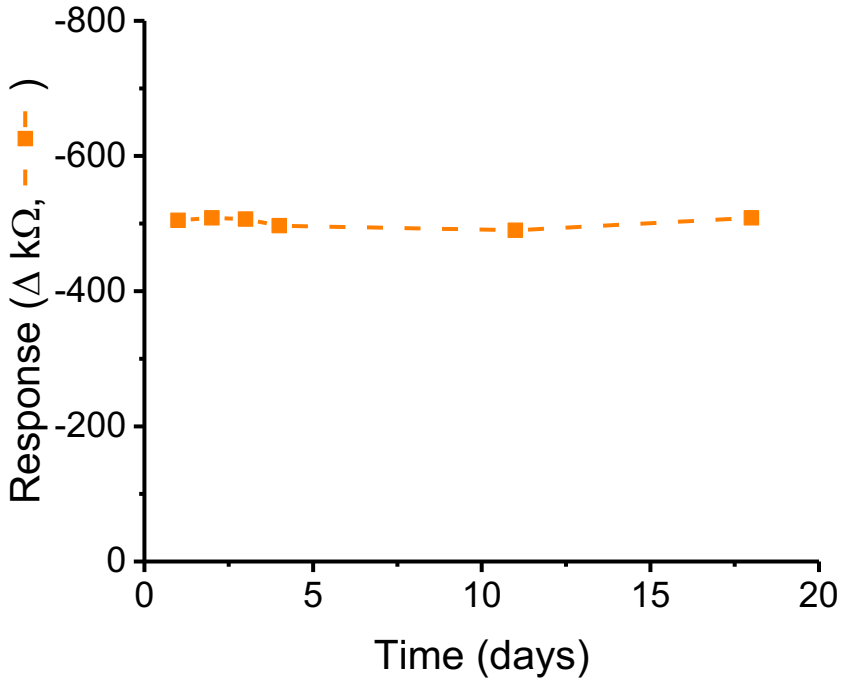

Figure 10: Stability of sensor toward 40.6% NH_3. Conditions: 100 $mmol.L^{-1}$ borate, 66 $mm.s^{-1}$ speed and 8.4 W power, pin-to-pin distance: 1.5 mm, pin width: 1.0 mm, carrier flow rate: 1 $sl.m^{-1}$, room temperature.

Lastly, the effect of the temperature selected for the operation of the sensor was investigated. This parameter is critically important for the development of gas sensors because it can affect the selectivity, sensitivity and response time. We first hypothesized that increasing the temperature of the sensor would give a faster response and recovery time. To determine the effects of temperature, the sensor was heated up to 100°C and it was found that the heat actually had the opposite effect on the sensor, the sensor showed no change in resistance when in the presence of NH_3 gas. To identify the roots of this behavior, the stability of the NADES was investigated using thermogravimetric analysis.

From that experiment, it was found that increasing the temperature caused the weight of the NADES to decrease drastically, as shown in Figure 11. This is data is shown to prove that the water is evaporating off once the temperature reaches 100°C over a period of time. This result was attributed to the release of the water in the NADES, component that was necessary to maintain the functionality of the solvent.

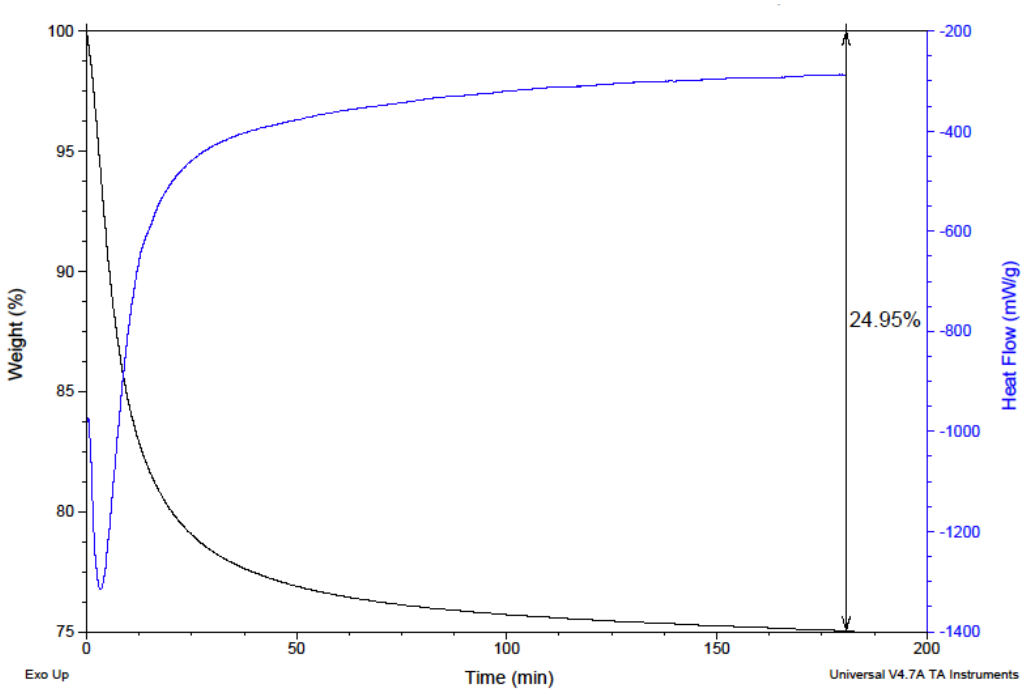

Figure 11: Isothermal TGA experiment with NADES.

2.5 Fish Spoilage Testing Using Gas Sensor.

As proof of the potential applications of the paper-derived sensor as a portable NH_3 sensor, we demonstrate its utility in the detection of NH_3 gas from the decaying of fish. Fish spoilage is a large issue in the food industry today. Spoiled fish not only has a bad smell but the generated biogenic amines can cause a wide range of health problems

including vomiting, diarrhea, hypotension, and edema. Among other compounds, spoiled fish samples are known to release NH_3, dimethylamine, and trimethylamine.[93] Thus, and as a proof of concept, the response of the sensor to a fish sample (Halibut, 1.0 g) left in a Falcon tube at room temperature was recorded and the results are shown in **Error! Reference source not found.**. As it can be observed, only a small response of the sensor (attributed to the release of NH_3 or possibly dimethylamine or trimethylamine) was observed during the first 12 hours. However, a much more significant response was observed beyond that time. **Error! Reference source not found.** also shows the estimated NH_3 concentration, calculated using the previously-described figures of merit (**Error! Reference source not found.**)

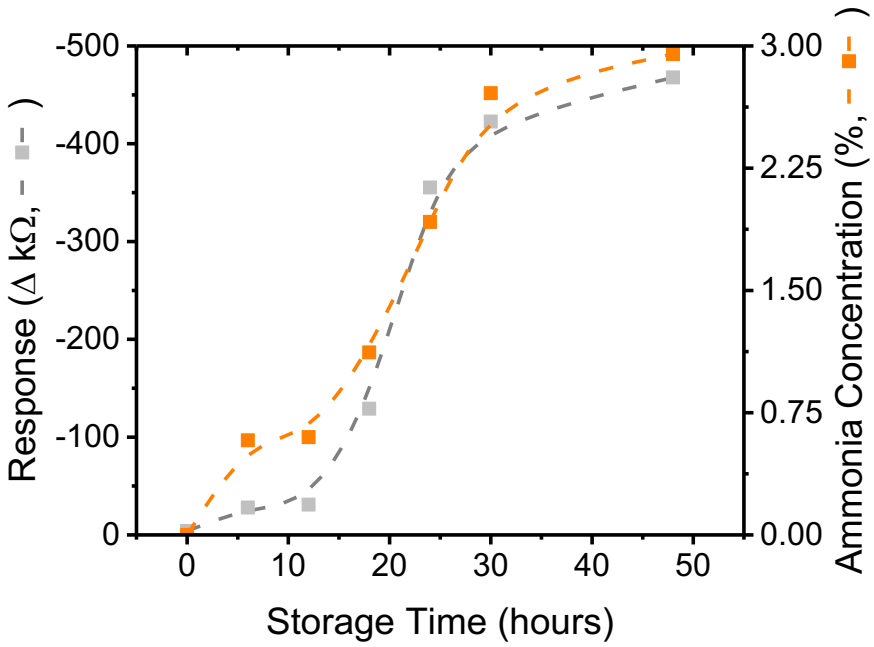

Figure 12: Sensor response toward Halibut as a function of storage time in 25 °C. Conditions: 100 mmol.L^{-1} borate, 66 mm.s^{-1} speed and 8.4 W power, pin-to-pin distance: 1.5 mm, pin width: 1.0 mm, carrier flow rate: 1 sl.m^{-1}, room temperature.

CHAPER THREE

CONCLUSIONS AND FUTURE RESEARCH

2. Conclusions of Paper-Derived Ammonia Gas Sensors

This report describes the first example for the integration of a paper-derived chemical sensor with NADES and its application to selectively quantify NH_3 in gas phase. The sensor was patterned using laser engraving and the conditions selected, to minimize the resistance of the material, by a chemometric approach. The sensor displayed very good selectivity towards NH_3, a limit of detection of 0.11%, and very good stability; enabling its application to follow the spoilage of a fish sample (Halibut), stored at room temperature. This new strategy to control selectivity using NADES could enable the development of many other gas sensors using (almost exclusively) organic materials, which despite of having lower sensitivity could address the need of emerging markets such as the NH_3-based fuel industry[94,95] or waste treatment[96] where most of the current sensors would be saturated.

2. Future Research

Without a question, the sensor developed has advantages over current technologies, including low-cost, simplicity and selectivity. That said, the current sensor is only able to measure the concentration of ammonia and the sensitivity need to be improved dramatically. To address these deficiencies, future research will be focused on the amount and functionality of the selected NADES. As a long-term goal, we believe the technology

developed could lead to the development of a multi-sensor array for multiple analytes, opening the door to inexpensive and simple tools for quality control in food or even biomedical applications.

REFERENCES

(1) Guerra, F. D.; Smith, G. D.; Alexis, F.; Whitehead, D. C. A Survey of VOC Emissions from Rendering Plants. *Aerosol Air Qual. Res.* **2017**, *17* (1), 209–217. https://doi.org/10.4209/aaqr.2016.09.0391.

(2) Ritz, C. W.; Fairchild, B. D.; Lacy, M. P. Implications of Ammonia Production and Emissions from Commercial Poultry Facilities: A Review. *J. Appl. Poult. Res.* **2004**, *13* (4), 684–692. https://doi.org/10.1093/JAPR/13.4.684.

(3) Mani, G. K.; Rayappan, J. B. B. A Highly Selective and Wide Range Ammonia Sensor - Nanostructured ZnO:Co Thin Film. *Mater. Sci. Eng. B Solid-State Mater. Adv. Technol.* **2015**, *191* (C), 41–50. https://doi.org/10.1016/j.mseb.2014.10.007.

(4) Talwar, V.; Singh, O.; Singh, R. C. ZnO Assisted Polyaniline Nanofibers and Its Application as Ammonia Gas Sensor. *Sensors Actuators, B Chem.* **2014**, *191*, 276–282. https://doi.org/10.1016/j.snb.2013.09.106.

(5) Mani, G. K.; Rayappan, J. B. B. A Highly Selective Room Temperature Ammonia Sensor Using Spray Deposited Zinc Oxide Thin Film. *Sensors Actuators, B Chem.* **2013**, *183*, 459–466. https://doi.org/10.1016/j.snb.2013.03.132.

(6) Timmer, B.; Olthuis, W.; Van Den Berg, A. Ammonia Sensors and Their Applications - A Review. *Sensors Actuators, B Chem.* **2005**, *107* (2), 666–677. https://doi.org/10.1016/j.snb.2004.11.054.

(7) Klotz, R. The Greenhouse Gas Emissions Consequences Of The Expanded Renewable Fuel Standard. **2010**.

(8) Sutton, M. A.; Erisman, J. W.; Dentener, F.; Möller, D. Ammonia in the Environment: From Ancient Times to the Present. *Environmental Pollution*. December 2008, pp 583–604. https://doi.org/10.1016/j.envpol.2008.03.013.

(9) Skjøth, C. A.; Geels, C. The Effect of Climate and Climate Change on Ammonia Emissions in Europe. *Atmos. Chem. Phys.* **2013**, *13* (1), 117–128. https://doi.org/10.5194/acp-13-117-2013.

(10) Nicolas-Debarnot, D.; Poncin-Epaillard, F. Polyaniline as a New Sensitive Layer for Gas Sensors. *Anal. Chim. Acta* **2003**, *475* (1–2), 1–15. https://doi.org/10.1016/S0003-2670(02)01229-1.

(11) Krupa, S. . Effects of Atmospheric Ammonia (NH3) on Terrestrial Vegetation: A Review. *Environ. Pollut.* **2003**, *124* (2), 179–221. https://doi.org/10.1016/S0269-7491(02)00434-7.

(12) Oudendag, D. A.; Luesink, H. H. The Manure Model: Manure, Minerals (N, P and K), Ammonia Emission, Heavy Metals and the Use of Fertiliser in Dutch Agriculture. *Nitrogen, the Confer-N-s* **1998**, 241–246. https://doi.org/10.1016/B978-0-08-043201-4.50037-X.

(13) Campbell, N. A.; Mitchell, L. G.; Reece, J. B.; Prepared, A.; Voss, C. H. *BIOLOGY: Concepts and Connections*; 2000.

(14) Kowalchuk, G. A.; Stephen, J. R. Ammonia-Oxidizing Bacteria: A Model for Molecular Microbial Ecology. *Annu. Rev. Microbiol.* **2001**, *55* (1), 485–529. https://doi.org/10.1146/annurev.micro.55.1.485.

(15) Steinfeld, H.; Gerber, P.; Wassenaar, T.; Castel, V.; Rosales, M.; de Haan, C.

Livestock's Long Shadow: Environmental Issues and Options; 2006.
(16) Oonincx, D. G. A. B.; van Itterbeeck, J.; Heetkamp, M. J. W.; van den Brand, H.; van Loon, J. J. A.; van Huis, A. An Exploration on Greenhouse Gas and Ammonia Production by Insect Species Suitable for Animal or Human Consumption. *PLoS One* **2010**, *5* (12). https://doi.org/10.1371/journal.pone.0014445.
(17) Wrage, N.; Velthof, G. L.; Van Beusichem, M. L.; Oenema, O. Role of Nitrifier Denitrification in the Production of Nitrous Oxide. *Soil Biology and Biochemistry*. Elsevier Ltd October 1, 2001, pp 1723–1732. https://doi.org/10.1016/S0038-0717(01)00096-7.
(18) Warneck, P. *Chemistry of the Natural Atmosphere*, 2nd Editio.; Academic Press, 1988.
(19) Erisman, J. W.; Otjes, R.; Hensen, A.; Jongejan, P.; Van Den Bulk, P.; Khlystov, A.; Möls, H.; Slanina, S.; Mok, H.; Slanina, S.; et al. Instrument Development and Application in Studies and Monitoring of Ambient Ammonia. *Atmos. Environ.* **2001**, *35* (11), 1913–1922. https://doi.org/10.1016/S1352-2310(00)00544-6.
(20) Bulgan, A. T. Use of Low Temperature Energy Sources in Aqua-Ammonia Absorption Refrigeration Systems. *Energy Convers. Manag.* **1997**, *38* (14), 1431–1438. https://doi.org/10.1016/0196-8904(95)00351-7.
(21) Colonna, P.; Gabrielli, S. Industrial Trigeneration Using Ammonia–Water Absorption Refrigeration Systems (AAR). *Appl. Therm. Eng.* **2003**, *23* (4), 381–396. https://doi.org/10.1016/S1359-4311(02)00212-0.
(22) Timmer, B.; Olthuis, W.; Berg, A. van den. Ammonia Sensors and Their Applications—a Review. *Sensors Actuators B Chem.* **2005**, *107* (2), 666–677. https://doi.org/10.1016/J.SNB.2004.11.054.
(23) Pijolat, C.; Pupier, C.; Sauvan, M.; Tournier, G.; Lalauze, R. Gas Detection for Automotive Pollution Control. *Sensors Actuators B Chem.* **1999**, *59* (2–3), 195–202. https://doi.org/10.1016/S0925-4005(99)00220-8.
(24) Oto, K.; Shinobe, A.; Manabe, M.; Kakuuchi, H.; Yoshida, Y.; Nakahara, T. New Semiconductor Type Gas Sensor for Air Quality Control in Automobile Cabin. *Sensors Actuators, B Chem.* **2001**, *77* (1–2), 525–528. https://doi.org/10.1016/S0925-4005(01)00717-1.
(25) Kim, Y. S.; Hwang, I. S.; Kim, S. J.; Lee, C. Y.; Lee, J. H. CuO Nanowire Gas Sensors for Air Quality Control in Automotive Cabin. *Sensors Actuators, B Chem.* **2008**, *135* (1), 298–303. https://doi.org/10.1016/j.snb.2008.08.026.
(26) Jun, Y. K.; Kim, H. S.; Lee, J. H.; Hong, S. H. CO Sensing Performance in Micro-Arc Oxidized TiO2 Films for Air Quality Control. *Sensors Actuators, B Chem.* **2006**, *120* (1), 69–73. https://doi.org/10.1016/j.snb.2006.01.045.
(27) Mount, G. H.; Rumburg, B.; Havig, J.; Lamb, B.; Westberg, H.; Yonge, D.; Johnson, K.; Kincaid, R. Measurement of Atmospheric Ammonia at a Dairy Using Differential Optical Absorption Spectroscopy in the Mid-Ultraviolet. *Atmos. Environ.* **2002**, *36* (11), 1799–1810. https://doi.org/10.1016/S1352-2310(02)00158-9.
(28) Hodgkinson, J.; Tatam, R. P. Optical Gas Sensing: A Review. *Meas. Sci. Technol* **2013**, *24*, 59. https://doi.org/10.1088/0957-0233/24/1/012004.

(29) Buttner, W. J.; Findlay, M.; Vickers, W.; Davis, W. M.; Cespedes, E. R.; Cooper, S.; Adams, J. W. In Situ Detection of Trinitrotoluene and Other Nitrated Explosives in Soils. *Anal. Chim. Acta* **1997**, *341* (1), 63–71. https://doi.org/10.1016/S0003-2670(96)00507-7.
(30) Carquigny, S.; Sanchez, J. B.; Berger, F.; Lakard, B.; Lallemand, F. Ammonia Gas Sensor Based on Electrosynthesized Polypyrrole Films. *Talanta* **2009**, *78* (1), 199–206. https://doi.org/10.1016/j.talanta.2008.10.056.
(31) Barsan, N.; Koziej, D.; Weimar, U. Metal Oxide-Based Gas Sensor Research: How To? *Sensors Actuators, B Chem.* **2007**, *121* (1), 18–35. https://doi.org/10.1016/j.snb.2006.09.047.
(32) Filipovic, L.; Selberherr, S. Performance and Stress Analysis of Metal Oxide Films for CMOS-Integrated Gas Sensors. *Sensors* **2015**, *15* (4), 7206–7227. https://doi.org/10.3390/s150407206.
(33) King, B. H.; Gramada, A.; Link, J. R.; Sailor, M. J. Internally Referenced Ammonia Sensor Based on an Electrochemically Prepared Porous SiO2 Photonic Crystal. *Adv. Mater.* **2007**, *19* (22), 4044–4048. https://doi.org/10.1002/adma.200602860.
(34) Liu, X.; Cheng, S.; Liu, H.; Hu, S.; Zhang, D.; Ning, H. A Survey on Gas Sensing Technology. *Sensors* **2012**, *12* (7), 9635–9665. https://doi.org/10.3390/s120709635.
(35) Kwak, D.; Lei, Y.; Maric, R. Ammonia Gas Sensors: A Comprehensive Review. *Talanta*. Elsevier B.V. November 1, 2019, pp 713–730. https://doi.org/10.1016/j.talanta.2019.06.034.
(36) James, D.; Scott, S. M.; Ali Ã, Z.; O, W. T.; Ali, Z.; O'Hare, W. T.; Ali Ã, Z.; O, W. T. Chemical Sensors for Electronic Nose Systems. *Microchim. Acta* **2005**, *149* (1), 1–17. https://doi.org/10.1007/s00604-004-0291-6.
(37) Warland, J. S.; Dias, G. M.; Thurtell, G. W. A Tunable Diode Laser System for Ammonia Flux Measurements over Multiple Plots. *Environ. Pollut.* **2001**, *114* (2), 215–221. https://doi.org/10.1016/S0269-7491(00)00218-9.
(38) Werle, P. W. Diode-Laser Sensors for In-Situ Gas Analysis. In *Laser in Environmental and Life Sciences*; Springer Berlin Heidelberg, 2004; pp 223–243. https://doi.org/10.1007/978-3-662-08255-3_11.
(39) Werle, P.; Slemr, F.; Maurer, K.; Kormann, R.; Mücke, R.; Jänker, B. Near- and Mid-Infrared Laser-Optical Sensors for Gas Analysis. *Opt. Lasers Eng.* **2002**, *37* (2–3), 101–114. https://doi.org/10.1016/S0143-8166(01)00092-6.
(40) Tittel, F. K.; Lewicki, R. Tunable Mid-Infrared Laser Absorption Spectroscopy. In *Semiconductor Lasers: Fundamentals and Applications*; Elsevier Ltd, 2013; pp 579–629. https://doi.org/10.1533/9780857096401.3.579.
(41) Michael, S.; Chow, W.; Schneider, H. Mid-Infrared Quantum-Dot Quantum Cascade Laser: A Theoretical Feasibility Study. *Photonics* **2016**, *3* (2), 29. https://doi.org/10.3390/photonics3020029.
(42) Wysocki, G.; Curl, R. F.; Tittel, F. K.; Maulini, R.; Bulliard, J. M.; Faist, J. Widely Tunable Mode-Hop Free External Cavity Quantum Cascade Laser for High Resolution Spectroscopic Applications. *Appl. Phys. B Lasers Opt.* **2005**, *81* (6),

769–777. https://doi.org/10.1007/s00340-005-1965-4.
(43) Maulini, R.; Yarekha, D. A.; Bulliard, J.-M.; Giovannini, M.; Faist, J.; Gini, E. Continuous-Wave Operation of a Broadly Tunable Thermoelectrically Cooled External Cavity Quantum-Cascade Laser. *Opt. Lett.* **2005**, *30* (19), 2584. https://doi.org/10.1364/ol.30.002584.
(44) Kosterev, A.; Wysocki, G.; Bakhirkin, Y.; So, S.; Lewicki, R.; Fraser, M.; Tittel, F.; Curl, R. F. Application of Quantum Cascade Lasers to Trace Gas Analysis. *Appl. Phys. B Lasers Opt.* **2008**, *90* (2), 165–176. https://doi.org/10.1007/s00340-007-2846-9.
(45) Tao, L.; Kang, ·; David, S. ·; Miller, J.; Pan, D.; Golston, L. M.; Zondlo, M. A. Low-Power, Open-Path Mobile Sensing Platform for High-Resolution Measurements of Greenhouse Gases and Air Pollutants. *Appl. Phys. B* **2015**, *119*, 153–164. https://doi.org/10.1007/s00340-015-6069-1.
(46) Kassim, A.; Basar, Z. B.; Mahmud, H. N. M. E. Effects of Preparation Temperature on the Conductivity of Polypyrrole Conducting Polymer. *Proc. Indian Acad. Sci. Chem. Sci.* **2002**, *114* (2), 155–162. https://doi.org/10.1007/BF02704308.
(47) Virji, S.; Huang, J.; Kaner, R. B.; Weiller, B. H. Polyaniline Nanofiber Gas Sensors: Examination of Response Mechanisms. *Nano Lett.* **2004**, *4* (3), 491–496. https://doi.org/10.1021/nl035122e.
(48) Gębicki, J.; Chachulski, B. Influence of Analyte Flow Rate on Signal and Response Time of the Amperometric Gas Sensor with Nafion Membrane. *Electroanalysis* **2009**, *21* (14), 1568–1576. https://doi.org/10.1002/elan.200804567.
(49) Bai, H.; Shi, G. Gas Sensors Based on Conducting Polymers. *Sensors* **2007**, *7* (3), 267–307. https://doi.org/10.3390/s7030267.
(50) de Araujo, W. R.; Frasson, C. M. R. R.; Ameku, W. A.; Silva, J. R.; Angnes, L.; Paixão, T. R. L. C. L. C.; de Araujo, W. R.; Frasson, C. M. R. R.; Ameku, W. A.; Silva, J. R.; et al. Single-Step Reagentless Laser Scribing Fabrication of Electrochemical Paper-Based Analytical Devices. *Angew. Chemie* **2017**, *129* (47), 15309–15313. https://doi.org/10.1002/anie.201708527.
(51) Yoon, H. Current Trends in Sensors Based on Conducting Polymer Nanomaterials. *Nanomaterials* **2013**, *3* (3), 524–549. https://doi.org/10.3390/nano3030524.
(52) Du, Z.; Li, C.; Li, L.; Yu, H.; Wang, Y.; Wang, T. Ammonia Gas Detection Based on Polyaniline Nanofibers Coated on Interdigitated Array Electrodes. *J. Mater. Sci. Mater. Electron.* **2011**, *22* (4), 418–421. https://doi.org/10.1007/s10854-010-0152-5.
(53) Andre, R. S.; Kwak, D.; Dong, Q.; Zhong, W.; Correa, D. S.; Mattoso, L. H. C.; Lei, Y. Sensitive and Selective NH3 Monitoring at Room Temperature Using ZnO Ceramic Nanofibers Decorated with Poly(Styrene Sulfonate). *Sensors (Switzerland)* **2018**, *18* (4). https://doi.org/10.3390/s18041058.
(54) Dey, A. Semiconductor Metal Oxide Gas Sensors: A Review. *Materials Science and Engineering B: Solid-State Materials for Advanced Technology*. Elsevier Ltd March 1, 2018, pp 206–217. https://doi.org/10.1016/j.mseb.2017.12.036.

(55) Prasad, A. K.; Gouma, P. I.; Kubinski, D. J.; Visser, J. H.; Soltis, R. E.; Schmitz, P. J. Reactively Sputtered MoO3 Films for Ammonia Sensing. In *Thin Solid Films*; Elsevier, 2003; Vol. 436, pp 46–51. https://doi.org/10.1016/S0040-6090(03)00524-8.
(56) Huang, J.; Wang, J.; Gu, C.; Yu, K.; Meng, F.; Liu, J. A Novel Highly Sensitive Gas Ionization Sensor for Ammonia Detection. *Sensors Actuators, A Phys.* **2009**, *150* (2), 218–223. https://doi.org/10.1016/j.sna.2009.01.008.
(57) Andre, R. S.; Chen, J.; Kwak, D.; Correa, D. S.; Mattoso, L. H. C.; Lei, Y. A Flexible and Disposable Poly(Sodium 4-Styrenesulfonate)/Polyaniline Coated Glass Microfiber Paper for Sensitive and Selective Detection of Ammonia at Room Temperature. *Synth. Met.* **2017**, *233*, 22–27. https://doi.org/10.1016/j.synthmet.2017.08.005.
(58) Chabanis, G.; Parkin, I. P.; Williams, D. E. Measurement Science and Technology Progress in the Development of Semiconducting Metal Oxide Gas Sensors: A Review Related Content Solid State Gas Sensors P T Moseley-A Simple Equivalent Circuit Model to Represent Microstructure Effects. **2017**. https://doi.org/10.1088/1361-6501/aa7443.
(59) Zeng, Y.; Lou, Z.; Wang, L.; Zou, B.; Zhang, T.; Zheng, W.; Zou, G. Enhanced Ammonia Sensing Performances of Pd-Sensitized Flowerlike ZnO Nanostructure. **2011**, *156* (1), 395–400. https://doi.org/10.1016/j.snb.2011.04.064.
(60) Zhang, D.; Jiang, C.; Li, P.; Sun, Y. Layer-by-Layer Self-Assembly of Co3O4 Nanorod-Decorated MoS2 Nanosheet-Based Nanocomposite toward High-Performance Ammonia Detection. *ACS Appl. Mater. Interfaces* **2017**, *9* (7), 6462–6471. https://doi.org/10.1021/acsami.6b15669.
(61) Wang, J. *Analytical Electrochemistry, Third Edition*; John Wiley and Sons: Hoboken, NJ, USA, 2006. https://doi.org/10.1002/0471790303.
(62) Rogers, E. I.; O'Mahony, A. M.; Aldous, L.; Compton, R. G. Amperometric Gas Detection Using Room Temperature Ionic Liquid Solvents. In *ECS Transactions*; ECS, 2010; Vol. 33, pp 473–502. https://doi.org/10.1149/1.3484806.
(63) Ji, X.; Banks, C. E.; Compton, R. G. The Electrochemical Oxidation of Ammonia at Boron-Doped Diamond Electrodes Exhibits Analytically Useful Signals in Aqueous Solutions. *Analyst* **2005**, *130* (10), 1345–1347. https://doi.org/10.1039/b508975a.
(64) Ji, X.; Silvester, D. S.; Aldous, L.; Hardacre, C.; Compton, R. G. Mechanistic Studies of the Electro-Oxidation Pathway of Ammonia in Several Room-Temperature Ionic Liquids. *J. Phys. Chem. C* **2007**, *111* (26), 9562–9572. https://doi.org/10.1021/jp0715732.
(65) Mu, X.; Wang, Z.; Zeng, X.; Mason, A. J. A Robust Flexible Electrochemical Gas Sensor Using Room Temperature Ionic Liquid. *IEEE Sens. J.* **2013**, *13* (10), 3976–3981. https://doi.org/10.1109/JSEN.2013.2262932.
(66) Sekhar, P. K.; Kysar, J. S. An Electrochemical Ammonia Sensor on Paper Substrate. *J. Electrochem. Soc.* **2017**, *164* (4), B113–B117. https://doi.org/10.1149/2.0941704jes.
(67) Espino, M.; de los Ángeles Fernández, M.; Gomez, F. J. V.; Silva, M. F. Natural

Designer Solvents for Greening Analytical Chemistry. *TrAC Trends Anal. Chem.* **2016**, *76*, 126–136. https://doi.org/10.1016/J.TRAC.2015.11.006.
(68) Karu, R.; Gedu, S.; Satyanarayana, G. Microwave Assisted Domino Heck Cyclization and Alkynylation: Synthesis of Alkyne Substituted Dihydrobenzofurans. *Green Chist.* **2018**, No. 20, 369–374. https://doi.org/10.1039/c7gc02606d.
(69) Gomez, F. J. V.; Espino, M.; Fernández, M. A.; Silva, M. F. A Greener Approach to Prepare Natural Deep Eutectic Solvents. *ChemistrySelect* **2018**, *3* (22), 6122–6125. https://doi.org/10.1002/slct.201800713.
(70) Dungchai, W.; Chailapakul, O.; Henry, C. S. Electrochemical Detection for Paper-Based Microfluidics. *Anal. Chem.* **2009**, *81* (14), 5821–5826. https://doi.org/10.1021/ac9007573.
(71) Amor-Gutiérrez, O.; Costa Rama, E.; Costa-García, A.; Fernández-Abedul, M. T. Paper-Based Maskless Enzymatic Sensor for Glucose Determination Combining Ink and Wire Electrodes. *Biosens. Bioelectron.* **2017**, *93*, 40–45. https://doi.org/10.1016/J.BIOS.2016.11.008.
(72) da Costa, T. H.; Song, E.; Tortorich, R. P.; Choi, J.-W. A Paper-Based Electrochemical Sensor Using Inkjet-Printed Carbon Nanotube Electrodes. *ECS J. Solid State Sci. Technol.* **2015**, *4* (10), S3044–S3047. https://doi.org/10.1149/2.0121510jss.
(73) Giuliani, J. G.; Benavidez, T. E.; Duran, G. M.; Vinogradova, E.; Rios, A.; Garcia, C. D. Development and Characterization of Carbon Based Electrodes from Pyrolyzed Paper for Biosensing Applications. *J. Electroanal. Chem.* **2016**, *765*, 8–15. https://doi.org/10.1016/J.JELECHEM.2015.07.055.
(74) Nine, M. J.; Tran, D. N. H.; Tung, T. T.; Kabiri, S.; Losic, D. Graphene-Borate as an Efficient Fire Retardant for Cellulosic Materials with Multiple and Synergetic Modes of Action. *ACS Appl. Mater. Interfaces* **2017**, *9* (11), 10160–10168. https://doi.org/10.1021/acsami.7b00572.
(75) Morgan, A. B.; Jurs, J. L.; Tour, J. M. Synthesis, Flame-Retardancy Testing, and Preliminary Mechanism Studies of Nonhalogenated Aromatic Boronic Acids: A New Class of Condensed-Phase Polymer Flame-Retardant Additives for Acrylonitrile–Butadiene–Styrene and Polycarbonate. *J. Appl. Polym. Sci.* **2000**, *76* (8), 1257–1268. https://doi.org/10.1002/(SICI)1097-4628(20000523)76:8<1257::AID-APP6>3.0.CO;2-#.
(76) Molton, P.; Demmitt, T. F. Reaction Mechanisms in Cellulose Pyrolysis: A Literature Review. *Battelle Pacific Northwest Lab.* **1977**, 49–50.
(77) Gabriel, E. F. M.; Coltro, W. K. T.; Garcia, C. D.; Moreira Gabriel, E. F.; Tomazelli Coltro, W. K.; Garcia, C. D.; Gabriel, E. F. M.; Coltro, W. K. T.; Garcia, C. D. *Fast and Versatile Fabrication of PMMA Microchip Electrophoretic Devices by Laser Engraving*; 2014; Vol. 35. https://doi.org/10.1002/elps.201300511.
(78) Hoa, N. D.; Van Quy, N.; Kim, D. Nanowire Structured SnOx-SWNT Composites: High Performance Sensor for NOx Detection. *Sensors Actuators, B Chem.* **2009**, *142* (1), 253–259. https://doi.org/10.1016/j.snb.2009.07.053.

(79) Chung, Y. M.; Halim, Z. A.; Raffay, R. Un-Ionized Ammonia Detection System for Water Quality Monitoring. In *2012 IEEE Asia-Pacific Conference on Applied Electromagnetics (APACE)*; IEEE, 2012; pp 274–279. https://doi.org/10.1109/APACE.2012.6457675.
(80) Cusano, A.; Consales, M.; Pisco, M.; Giordano, M.; Viter, R.; Campopiano, S.; Smyntyna, V. A Novel Optochemical Sensor Based on SnO2 Sensitive Thin Film for Ppm Ammonia Detection in Liquid Environment. *J. Light. Technol. Vol. 24, Issue 12, pp. 5000-5007* **2006**, *24* (12), 5000–5007.
(81) Papadopoulou, E. L.; Morselli, D.; Prato, M.; Barcellona, A.; Athanassiou, A.; Bayer, I. S. An Efficient Pure Polyimide Ammonia Sensor. *J. Mater. Chem. C* **2016**, *4*, 7790. https://doi.org/10.1039/c6tc02375d.
(82) Tang, Y.; Zhou, D.; Zhang, J.; Zhu, X. Fabrication and Properties of Paper Coatings with the Incorporation of Nanoparticle Pigments: Rheological Behavior. *Dig. J. Nanomater. Biostructures* **2013**, *8* (4), 1699–1710.
(83) Bundy, W. M.; Ishley, J. N. Kaolin in Paper Filling and Coating. *Appl. Clay Sci.* **1991**, *5* (5–6), 397–420. https://doi.org/10.1016/0169-1317(91)90015-2.
(84) Burnham, A. K.; Zhou, X.; Broadbelt, L. J. Critical Review of the Global Chemical Kinetics of Cellulose Thermal Decomposition. *Energy and Fuels*. American Chemical Society May 2015, pp 2906–2918. https://doi.org/10.1021/acs.energyfuels.5b00350.
(85) Lin, Y.-C.; Cho, J.; Tompsett, G. A.; Westmoreland, P. R.; Huber, G. W. Kinetics and Mechanism of Cellulose Pyrolysis. *J. Phys. Chem. C* **2009**, *113* (46), 20097–20107. https://doi.org/10.1021/jp906702p.
(86) Mcdonald-Wharry, J. S.; Manley-Harris, M.; Pickering, K. L. Reviewing, Combining, and Updating the Models for the Nanostructure of Non-Graphitizing Carbons Produced from Oxygen-Containing Precursors. **2016**. https://doi.org/10.1021/acs.energyfuels.6b00917.
(87) Konermann, L. Addressing a Common Misconception: Ammonium Acetate as Neutral PH “Buffer” for Native Electrospray Mass Spectrometry. *J. Am. Soc. Mass Spectrom.* **2017**, *28* (9), 1827–1835. https://doi.org/10.1007/s13361-017-1739-3.
(88) Maity, A.; Raychaudhuri, A. K.; Ghosh, B. High Sensitivity NH3 Gas Sensor with Electrical Readout Made on Paper with Perovskite Halide as Sensor Material. *Sci. Rep.* **2019**, *9* (1), 7777. https://doi.org/10.1038/s41598-019-43961-6.
(89) Cui, S.; Pu, H.; Lu, G.; Wen, Z.; Mattson, E. C.; Hirschmugl, C.; Gajdardziska-Josifovska, M.; Weinert, M.; Chen, J. Fast and Selective Room-Temperature Ammonia Sensors Using Silver Nanocrystal-Functionalized Carbon Nanotubes. *ACS Appl. Mater. Interfaces* **2012**, *4*, 4898−4904. https://doi.org/10.1021/am301229w.
(90) Vaughan, A. A.; Baron, M. G.; Narayanaswamy, R. Optical Ammonia Sensing Films Based on an Immobilized Metalloporphyrin. *Anal. Commun.* **1996**, *33* (11), 393–396. https://doi.org/10.1039/ac9963300393.
(91) Shang, Y.; Wang, X.; Xu, E.; Tong, C.; Wu, J. Optical Ammonia Gas Sensor Based on a Porous Silicon Rugate Filter Coated with Polymer-Supported Dye. *Anal. Chim. Acta* **2011**, *685* (1), 58–64. https://doi.org/10.1016/j.aca.2010.11.008.

(92) Ugur, I.; Marion, A.; Parant, S.; Jensen, J. H.; Monard, G. Rationalization of the PKa Values of Alcohols and Thiols Using Atomic Charge Descriptors and Its Application to the Prediction of Amino Acid PKa's. *J. Chem. Inf. Model.* **2014**, *54* (8), 2200–2213. https://doi.org/10.1021/ci500079w.
(93) Jensen, B. B.; Engberg, R. M. *Encyclopedia of Meat Sciences*; Elsevier, 2004. https://doi.org/10.1016/B0-12-464970-X/00030-1.
(94) Nam, J. Y.; Kim, H. W.; Shin, H. S. Ammonia Inhibition of Electricity Generation in Single-Chambered Microbial Fuel Cells. *J. Power Sources* **2010**, *195* (19), 6428–6433. https://doi.org/10.1016/j.jpowsour.2010.03.091.
(95) Valera-Medina, A.; Marsh, R.; Runyon, J.; Pugh, D.; Beasley, P.; Hughes, T.; Bowen, P. Ammonia–Methane Combustion in Tangential Swirl Burners for Gas Turbine Power Generation. *Appl. Energy* **2017**, *185*, 1362–1371. https://doi.org/10.1016/j.apenergy.2016.02.073.
(96) Bermejo, M. D.; Cantero, F.; Cocero, M. J. Supercritical Water Oxidation of Feeds with High Ammonia Concentrations. Pilot Plant Experimental Results and Modeling. *Chem. Eng. J.* **2008**, *137* (3), 542–549. https://doi.org/10.1016/j.cej.2007.05.010.